FULL PAPERS

Magnetic Resonance in Medicine 58:931–938 (2007)

Wideband SSFP: Alternating Repetition Time Balanced Steady State Free Precession with Increased Band Spacing

Krishna S. Nayak,[1]* Hsu-Lei Lee,[1] Brian A. Hargreaves,[2] and Bob S. Hu[3]

Balanced steady-state free precession (SSFP) imaging is limited by off-resonance banding artifacts, which occur with periodicity 1/TR in the frequency spectrum. A novel balanced SSFP technique for widening the band spacing in the frequency response is described. This method, called wideband SSFP, utilizes two alternating repetition times with alternating RF phase, and maintains high SNR and T_2/T_1 contrast. For a fixed band spacing, this method can enable improvements in spatial resolution compared to conventional SSFP. Alternatively, for a fixed readout duration this method can widen the band spacing, and potentially avoid the banding artifacts in conventional SSFP. The method is analyzed using simulations and phantom experiments, and is applied to the reduction of banding artifacts in cine cardiac imaging and high-resolution knee imaging at 3T. Magn Reson Med 58:931–938, 2007. © 2007 Wiley-Liss, Inc.

Key words: balanced SSFP; banding artifacts; alternating repetition time; oscillating steady states; MRI pulse sequence

INTRODUCTION

Balanced steady state free precession (SSFP, also known as True-FISP, FIESTA, or Balanced-FFE) has emerged as a powerful technique for rapid magnetic resonance imaging. Compared to gradient-echo techniques, SSFP provides superior SNR efficiency and image quality, but is highly sensitive to resonance frequency (1–4). In particular, the usable bandwidth of conventional SSFP is less than 1/TR. Signal nulls occur every 1/TR in resonance frequency, producing well-known "banding" artifacts in images. More global transient artifacts occur when bands fall in regions of flow (5).

In static tissue, multiple-acquisition methods using phase-cycling (4,6,7) successfully eliminate banding, but require multiple steady-states to be reached, and increase scan-time by at least a factor of two. Banding can also be avoided by shortening the TR (8). However, this reduces the maximum readout duration and limits spatial resolution. Shortening the TR also reduces the readout duty-cycle, and hence SNR efficiency, and may prevent the use of time-efficient k-space trajectories such as echo-planar (9,10) or spiral (11).

The hypothesis of this work is that alternating repetition times can be used to widen band-spacing of SSFP beyond 1/TR, and therefore reduce and potentially avoid banding artifacts in single-acquisition SSFP MRI. This technique, called wideband SSFP, uses two alternating repetition times (12) with alternating RF phase to establish a band spacing that is up to two times wider than that of conventional SSFP, with a modest increase in scan-time (13).

We first present a theoretical description of wideband SSFP and the mechanism for increasing band spacing, and analytic approximations for the resulting image contrast and SNR efficiency compared to conventional SSFP. Simulations are used to accurately determine the image contrast, optimal flip angle, and SNR efficiency of wideband SSFP. Wideband SSFP signal profiles are verified in a phantom study. Finally, the proposed method is applied in vivo to banding artifact reduction in cine ventricular function imaging and high-resolution cartilage imaging at 3 Tesla.

THEORY

The SSFP pulse sequence consists of a rapidly repeating sequence of fully balanced excitations and acquisitions. All gradients have zero net area over the course of one repetition ($\int_0^{TR} \bar{G}(t)dt = 0$), and should also have a zero gradient first-moment when imaging in areas of flow ($\int_0^{TR} \bar{G}(t)tdt = 0$) (11). Compared to gradient echo techniques, balanced SSFP provides superior SNR efficiency and strong T_2/T_1 contrast. For these reasons, balanced SSFP has proved useful in many cardiovascular, neurologic, body, and musculoskeletal applications.

One of two primary drawbacks of SSFP (the other one is RF heating) is its sensitivity to resonance frequency (1–4), with signal nulls occurring every 1/TR. These signal nulls often obscure anatomical structures, cause global artifacts due to transient oscillations and flow (5,14,15) and reduce the dianostic image quality.

Alternating-TR SSFP

Alternating the repetition time (TR) between two values with appropriate phase-cycling, has been successfully used to modify the spectral response of SSFP, and has been demonstrated as a means for achieving fat suppression (12, 16). The aim of this work is to use alternating-TR to widen

[1]Magnetic Resonance Engineering Laboratory, Ming Hsieh Department of Electrical Engineering, University of Southern California, Los Angeles, California
[2]Department of Radiology, Stanford University, Stanford, California
[3]Department of Cardiovascular Medicine, Palo Alto Medical Foundation, Palo Alto, California

Grant sponsor: National Institutes of Health; Grant Number: R21-HL079987; Grant sponsor: American Heart Association; Grant number: 0435249N; Grant sponsors: James H. Zumberge Foundation, GE Healthcare.

A preliminary version of this work was presented at the ISMRM 13th Scientific Sessions in May 2005 (Abstract #2387, 1st place best poster award in the category "Pulse Sequences").

*Correspondence to: Krishna S. Nayak, 3740 McClintock Ave, EEB 406, Los Angeles, CA 90089 - 2564. E-mail: knayak@usc.edu

Received 6 August 2006; revised 5 April 2007; accepted 8 April 2007.

DOI 10.1002/mrm.21296
Published online in Wiley InterScience (www.interscience.wiley.com).

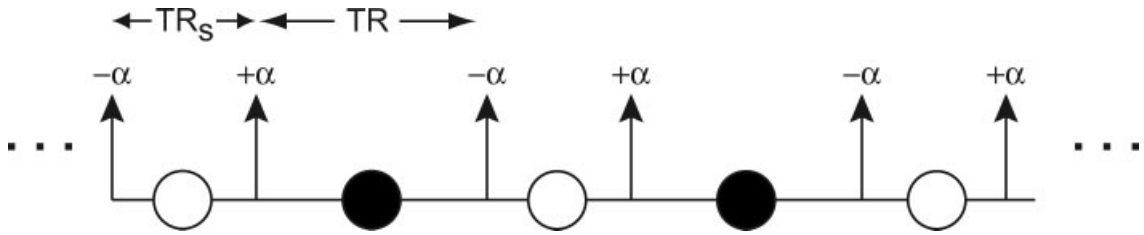

FIG. 1. An idealized wideband SSFP pulse sequence, which uses alternating repetition times, TR and TR_s, with alternating RF sign, and fully balanced gradients between each pair of RF pulses.

the band spacing of SSFP and minimize undesired signal nulling (13). This technique is referred to as wideband SSFP, and is illustrated in Fig. 1. Two alternating repetition times (TR_s and TR) with alternating RF phase are used to produce an oscillating steady state with two distinct echoes (black and white circles). The primary design parameter is the ratio of the short and long repetition times, which we define as $a = TR_s/TR$, where $0 < a \leq 1$. Both echoes may be used for imaging, however, as a becomes small, it may be impractical to acquire data during TR_s (white circle). Note that when $a = 1$, this sequence is equivalent to conventional SSFP.

Mechanism for Increasing the Band Spacing

Figure 2 illustrates the steady-state magnetization path and frequency response of wideband SSFP with $a = 1.0, 0.7$, and 0.4. Five isochromats are shown, exhibiting different amounts of precession during TR: 0.1π, 0.3π, 0.5π, 0.7π, and 0.9π. In conventional SSFP ($a = 1.0$, Fig. 2a–c), precession and relaxation are the same in both TR intervals, resulting in a symmetric steady-state. As the precession over a TR approaches π, the steady-state magnetization and signal approaches zero, which produces the well-known "banding" artifact in SSFP MRI (1,3) at resonance frequencies $\frac{1}{2TR}$, $-\frac{1}{2TR}$, and periodically thereafter.

Wideband SSFP tilts the magnetization path to one side (see Fig. 2d–i), permitting a greater amount of precession during TR before signal nulling occurs. The precession over TR can be greater than π and the net deflection (along Mx in Fig. 2) will still be balanced by correspondingly smaller amounts of precession during TR_s. The echo during TR (black circle, solid black profile) has a wide flat passband with all depicted isochromats exhibiting nearly identical transverse magnetization, therefore producing uniform signal. The echo during TR_s (white circle, dashed green profile) has higher and less-uniform signal across the passband.

Band Spacing of Wideband SSFP

The null-to-null spacing as a function of a is shown in Fig. 3. The band spacing is not a function of T_2/T_1, but does depend on flip angle, α. As α is reduced, the band spacing approaches $\frac{2}{TR(1+a)}$ or equivalently, $\frac{2}{TR+TR_s}$. This empirical approximation is used for the remainder of this manuscript and has an error of less than 5% for $\alpha < 60°$, where error is measured as the difference between the approximated band spacing and true band spacing divided by the true band spacing.

The ability of this method to modify the SSFP frequency response is illustrated in Fig. 4. For a fixed imaging TR, wideband SSFP can be used to widen the band spacing (see Fig. 4a). As TR_s is shortened (with TR fixed), there is a decrease in signal intensity and a widening of the passband. In this way, wideband SSFP may be used to reduce and potentially avoid banding artifacts. For a fixed band spacing, wideband SSFP can be used to increase the available readout duration (see Fig. 4b) As TR is increased (with TR + TR_s fixed), there is a decrease in signal intensity but the passband width is maintained. In this way, wideband SSFP may be used to increase the available readout duration and (1) achieve high spatial resolution, which is limited by the amount of gradient area that will fit within TR, or (2) use time-efficient readout schemes (9–11).

Image Contrast

The steady state magnetization at the imaging echo can be derived analytically from the Bloch equations in matrix form (17). On-resonance, the magnitude of the transverse magnetization in the steady state simplifies to:

$$|M_{xy}| = \frac{\left[(a+\cos\alpha)\frac{T_1}{T_2} + (1 - a\cos\alpha)\right]\sin\alpha}{\sin^2\alpha\left(1-\frac{T_1}{T_2}\right)^2 + \frac{T_1}{T_2}\left(\sqrt{a}+\frac{1}{\sqrt{a}}\right)^2} \quad [1]$$

Note that when $a = 1.0$ (conventional SSFP), this is equivalent to Eq. [12] from Ref. 18. When $\alpha = 90°$, Eq. [1] simplifies to:

$$|M_{xy}| \approx \frac{aT_2}{T_1 + aT_2} = \frac{a\frac{T_2}{T_1}}{1 + a\frac{T_2}{T_1}} \quad [2]$$

This suggests that wideband SSFP exhibits T_2/T_1-like contrast similar to that of conventional balanced SSFP.

Numerical Bloch simulation can be used to determine the contrast over the relevant range of resonance offsets. Figure 5 illustrates the steady-state passband signal as a function of T_2/T_1, for different a-values and approximately the same band spacing (i.e. with TR + TR_s fixed). The plotted signal amplitude is relative to M_o, and is an average over 2/3 of the null-to-null spacing in the spectral profile of each sequence. Smaller a-values generate weaker signal and contrast during TR and stronger signal and contrast during TR_s.

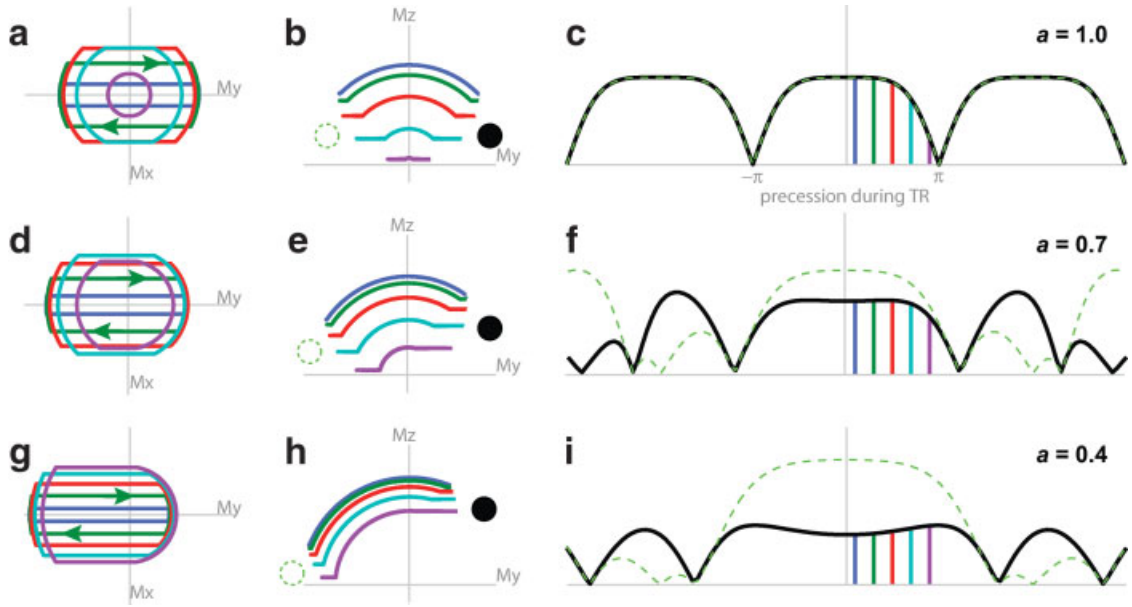

FIG. 2. The steady-state magnetization path and signal profiles during conventional and wideband SSFP. Paths for five isochromats with different amounts of precession during the imaging TR (blue, 0.1π; green, 0.3π; red, 0.5π; cyan, 0.7π; purple, 0.9π) are shown (left column) in the x, y plane and (middle column) in the y, z plane. The echo during the imaging TR is shown by the black circle (middle column) and the solid black signal profile (right column). The echo during TR_s is shown by the white circle (middle column) and dashed green signal profile (right column). Simulations correspond to $T_1 = T_2 \gg$ TR, $\alpha = 90°$, and excitations along the x-axis. In conventional balanced SSFP, precession and relaxation are the same in both TR intervals, resulting in a symmetric steady-state. In wideband SSFP, the path is tilted towards one side, enabling a greater amount of precession during TR before banding occurs. Notice that during TR (black circle), the transverse magnetization (black line) in wideband SSFP is nearly identical for all isochromats shown, when $a = 0.7$ and 0.4.

Optimal Flip Angle for Wideband SSFP

The choice of imaging flip angle is typically made to maximize SNR efficiency while operating within SAR limits. The steady-state signal is a function of both a and α, and therefore the SNR or CNR optimal flip angle will vary with α. Figure 6 illustrates the myocardial ($T_1/T_2 =$ 1100/40 msec) and blood ($T_1/T_2 = 1500/140$ msec) signal at 3T for different flip angles and a-values. Notice that the optimal flip angle for wideband SSFP is comparable to that of conventional SSFP when $a > 0.3$.

Central Signal Dip

The signal profile of wideband SSFP exhibits an intrinsic signal dip close to on-resonance ($\Delta f = 0$) when relaxation and other phase effects become significant relative to precession (see Fig. 7). Our empirical observations are that the size of the dip is a function of T_2/T_1 (deeper for lower ratios), and the width of the dip is a function of absolute T_2/TR and T_1/TR (widens for lower values). For the 3T cardiac study parameters described below, the signal dip size is 3.6% and 4.1% for myocardium and blood, respectively. Although small, such a dip may appear as a narrow signal band in tissues exactly on-resonance, and may cause mild transient artifacts if there is flow or motion through this region.

SNR Efficiency

The SNR efficiency of wideband SSFP depends heavily on whether one or both echoes are used, and on the duration of excitation and other pulses that influence the available readout duration. As the a-value is reduced, the signal during TR decreases (see Eq. [2]) and the signal during TR_s increases. Here, we consider the relative SNR efficiency of wideband SSFP in the case where TR_s is not used for data collection.

Considering the conservative case where only TR is used for imaging, and comparing wideband SSFP with conventional SSFP with the same TR: (1) the scan-time is $(1 + a)$ times longer, and (2) the passband signal is lowered by a

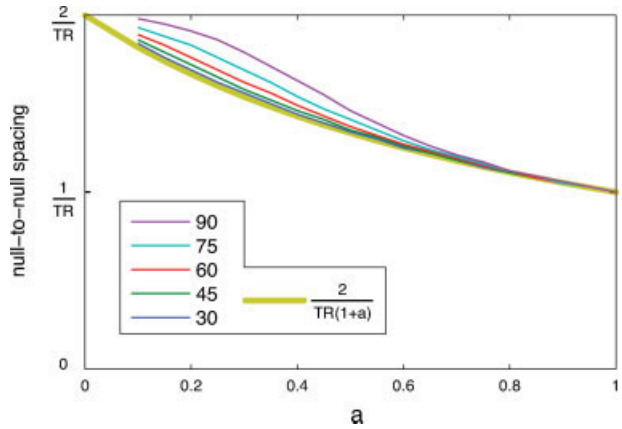

FIG. 3. Wideband SSFP null-to-null band spacing as a function of the TR asymmetry, a, for various flip angles. As flip angle is reduced, the band spacing approaches $\frac{2}{TR(1+a)}$. The band spacing is independent of T_2/T_1.

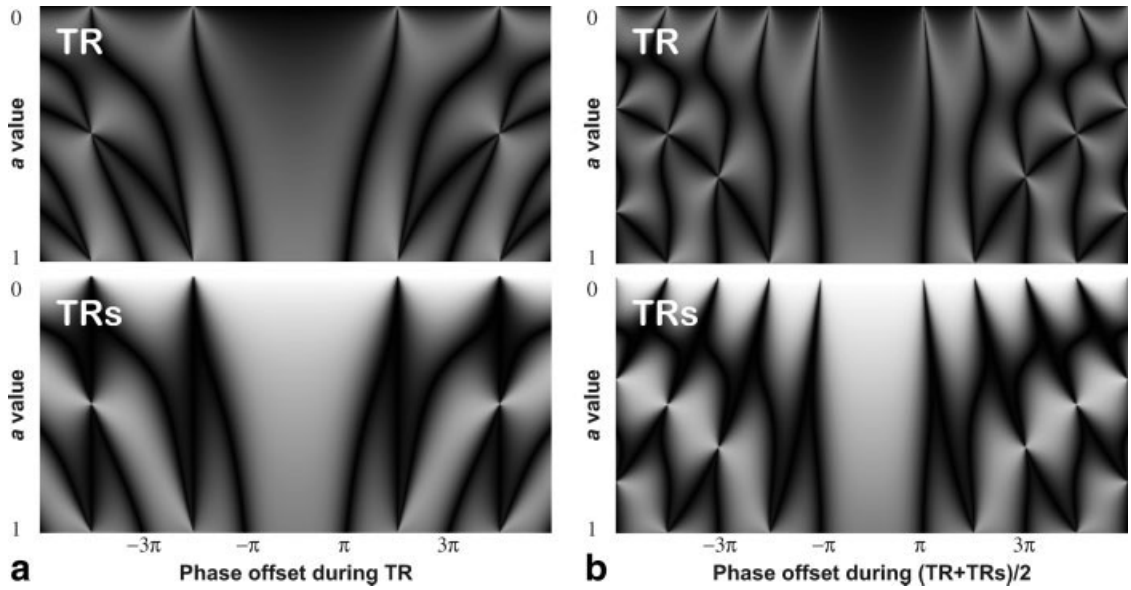

FIG. 4. Wideband SSFP signal profiles for (**a**) fixed TR, and (**b**) approximately fixed band spacing (fixed TR+TR_s). Signal responses during TR (top) and TR_s (bottom) are shown. The horizontal axis represents precession due to off-resonance. (**a**) Lower *a*-values increase the band spacing. (**b**) Lower *a*-values correspond to longer TR, and therefore longer available readout time. The bottom line of each image represents conventional SSFP, and the bands at $\pm 2k\pi$ (integer $k \geq 1$) disappear. Profiles correspond to $\alpha = 90^\circ$ and $T_2 = T_1 \gg$ TR.

factor, called S. As such, the resulting SNR efficiency would be:

$$\frac{\mu_w}{\mu_c} = \frac{S}{\sqrt{1+a}} \quad [3]$$

where μ_w and μ_c represent the SNR efficiency of wideband and conventional SSFP, respectively, and μ is defined as $\frac{\text{SNR}}{\Delta v\sqrt{T_{scan}}}$, Δv is the voxel size, and T_{scan} is the total scan time. Note that S is always less than 1, even when using the optimal flip angle for wideband SSFP (see Fig. 6). The SNR efficiency of wideband SSFP (when used to avoid banding artifacts) is always lower than that of conventional SSFP. In static imaging scenarios, where multiple-NEX are needed to achieve adequate SNR, multiple-acquisition methods will remain the method of choice for removing banding artifacts (4,6,7), because of their SNR efficiency. In cases where multiple acquisition methods are not applicable, or where SNR can be traded for reduced banding (common in high-field SSFP imaging), wideband SSFP will be faster than multiple-acquisition methods by a factor of at least $2/(1+a)$.

Considering the case where only TR is used for imaging, and comparing wideband SSFP with conventional SSFP with the same approximate band spacing (i.e. TR = $\frac{2}{1+a}TR_c$, where TR_c is the repetition time of conventional SSFP): (1) the scan-time is two times longer, (2) the passband signal is lowered by a factor S, and (3) the available readout duration is increased by a factor x. The resulting SNR efficiency would be:

$$\frac{\mu_w}{\mu_c} = S\sqrt{\frac{x}{2}} \quad [4]$$

by defining T_d as the amount of time per TR that is not usable for data acquisition, x can be expressed as:

$$x = \frac{TR - T_d}{TR_c - T_d} \quad [5]$$

where TR and TR_c are the repetition times for wideband and conventional SSFP, respectively. In this case, the SNR efficiency of wideband SSFP will be superior to that of conventional SSFP when T_d is a substantial fraction of TR_c, therefore making x large. This can be the case in high-field imaging applications where the TR_c is limited to a few milliseconds because of off-resonance effects within a region of interest.

Initial Preparation

Accelerating the approach to steady state is important when combining this technique with any type of contrast preparation (e.g. fat saturation or inversion recovery). The single "$\alpha/2$" tip approach (19) can be easily adapted to align the direction of $\vec{M}$ with the steady-state magnetization at the echo during either TR or TR_s. The excitation angle should be the angle between the steady-state magnetization at the echo and the longitudinal axis, which for wideband SSFP, is a function of both α and a. Figure 8 illustrates the simulated reduction in transient oscillations for myocardium at 3T, when using a single tip preparatory pulse to tilt $\vec{M}$ to the axis of $\vec{M}_{ss}$ during TR.

MATERIALS AND METHODS

Experiments were performed on a Signa Excite HD 3T scanner (GE Healthcare, Waukesha, WI) with gradients capable

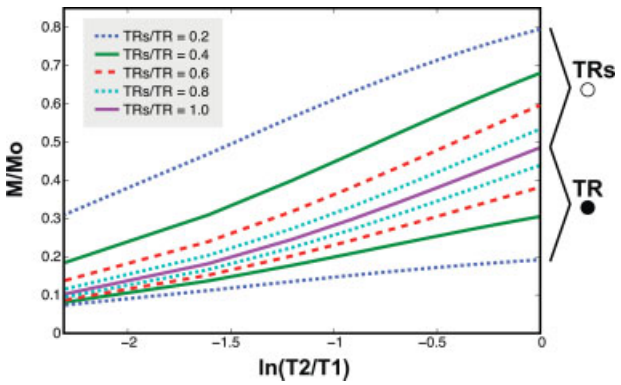

FIG. 5. Wideband SSFP signal as a function of T_2/T_1 for different a-values. The plotted signal, M/M_o, is an average over 2/3 of the null-to-null spacing in the spectral profile of each sequence. (upper lines) Signal during TR_s. (lower lines) Signal during TR.

of 40 mT/m amplitude and 150 mT/m/msec slew rate, and receiver capable of ±250 kHz bandwidth (2 μsec sampling). In phantom studies, a transmit/receive birdcage head coil was used. In cardiac studies, the body coil was used for transmission, and an 8-channel cardiac phased array was used for signal reception. In knee studies, the body coil was used for transmission and a 5-inch surface coil was used for signal reception. Scan volunteers provided written informed consent, and the imaging protocol was approved by our institutional review board.

A phantom study was performed to measure the spectral response and band-spacing of wideband SSFP. A uniform ball phantom ($T_1/T_2 \approx 150/30$ msec) was imaged with centered 2DFT readouts during both echoes. A linear shim was applied along the frequency-encoding direction to create in-plane off-resonance. The scan parameters were flip angle = 30°, TR = 6 msec, and a=1.0, 0.75, and 0.5. The measured spectral response was compared with Bloch simulations performed using MATLAB (Mathworks, South Natick, MA). Simulations used the actual gradient and RF waveforms from the experiments, and utilized the hard-pulse approximation with 4 μsec timesteps (17).

Wideband SSFP was applied to breath-held gated CINE cardiac imaging in three healthy volunteers. Localized center-frequency adjustment was performed over the left ventricle, and short-axis scan-planes were prescribed. Imaging parameters were: 2DFT acquisition, FOV = 30 × 30 cm^2, resolution = 1.2 × 1.2 × 8 mm^3, α = 30°, TR = 4.4 msec, plethysmograph gating, 16 R-R breath-hold. Data was acquired using conventional SSFP (a = 1) resulting in a temporal resolution of 76.8 msec, and with wideband SSFP (a = 0.45) resulting in a temporal resolution of 115.2 msec. In the case of wideband SSFP, no data was collected during TR_s resulting in the lower temporal resolution. The expected band spacing for conventional and wideband acquisitions was 227 Hz and 313 Hz, respectively.

Wideband SSFP was applied to slice-selective knee imaging in two healthy volunteers. Imaging parameters were: 2DFT acquisition, FOV = 15 × 15 cm^2, low resolution = 0.3 × 0.3 × 5 mm^3, high resolution = 0.15 × 0.3 × 5 mm^3. Data was acquired using low resolution conventional SSFP (a = 1, α = 25°, 10 sec scan time), high resolution conventional SSFP (a = 1, α = 22°, 22 sec scan time), and high resolution wideband SSFP (a = 0.26, α = 31°, 35 sec scan time). The flip angle choice was optimized for cartilage. In the case of wideband SSFP, no data was collected during TR_s.

RESULTS

Figure 9 contains images and signal profiles from the phantom experiment. The band spacing in simulated and measured spectral responses showed excellent agreement. The measured null-to-null spacing of wideband SSFP with a = 0.75 and a = 0.5 were 11 and 34% larger than conventional SSFP (a = 1.0). As expected, the signal intensity of the long TR echo was observed to be lower than that of the short TR echo.

Figure 10 contains 3T cardiac images from one representative study. Conventional SSFP images exhibited banding artifacts (white arrow) and transient artifacts. When viewing these data in a cine loop, it is clear that the transient artifacts are due to flow. In all studies, wideband SSFP

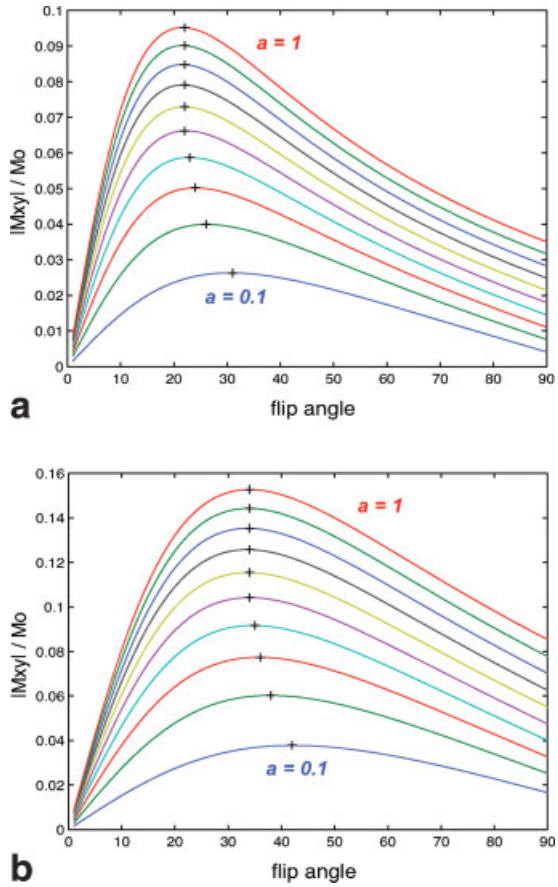

FIG. 6. Optimal flip angle for wideband SSFP. Steady-state signal as a function of a and α for (**a**) myocardium T_1/T_2 = 1100/40 msec, and blood T_1/T_2 = 1500/140 msec at 3T. The curves reflect a-values of 1.0 (highest) to 0.1 (lowest) with an increment of 0.1. The peak signal for each curve is marked with a "+". The optimal flip angle of wideband SSFP is comparable to that of conventional SSFP when $a > 0.3$. [Color figure can be viewed in the online issue, which is available at www.interscience.wiley.com.]

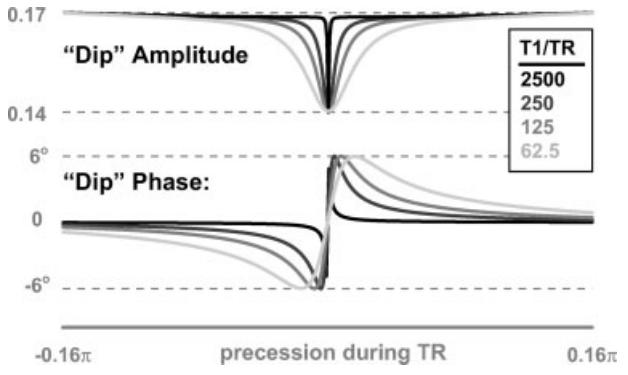

FIG. 7. Illustration of the intrinsic central dip in the wideband SSFP signal profile for $a = 0.5$, $T_2 = 0.3T_1$, and $T_1/\mathrm{TR} = 2500, 250, 125$, and 62.5. The dip widens for lower T_1/TR, and is small in both amplitude and phase. For the 3T cardiac study described later (see Fig. 10), the maximum signal dip is 3.6% and 5.1% for myocardium and blood, respectively.

successfully widened the band spacing, shifted the banding artifact outside of the heart, and reduced flow-related transient artifacts, presumably due to the uniformity of the wideband SSFP signal profile. As expected, the wideband SSFP images show slightly reduced blood-myocardium contrast compared to conventional SSFP.

Figure 11 contains 3T knee images from one representative study. Low resolution SSFP images were free of banding artifacts, while high-resolution SSFP experienced banding artifacts (white arrows) due to the required increase in readout length and increase in TR. Wideband SSFP successfully suppressed the banding artifact, and exhibited the expected high spatial resolution compared to low-resolution SSFP with the same band spacing.

DISCUSSION

We have demonstrated that alternating repetition times can be used to widen the band spacing in the frequency response of SSFP. For a fixed readout duration (motivated by the desired spatial resolution, or a particular acquisition) wideband SSFP increases the null-to-null spacing in the steady-state frequency response, thereby reducing and potentially avoiding banding artifacts. This has been successfully applied to cine ventricular function imaging and cartilage imaging at 3 Tesla.

Instead, for a fixed band spacing requirement (motivated by off-resonance in a region-of-interest) this approach increases the available readout duration. This can enable higher spatial resolution in applications such as 3T SSFP coronary artery imaging, and can permit the use of time-efficient k-space trajectories such as echo-planar (9,10) or spiral (11), which have been used for cardiac imaging at 1.5T.

Wideband SSFP may also be appropriate for clinical applications that fundamentally cannot be achieved using multiple-acquisition methods. MR fluoroscopy (continuous imaging) is one such example that requires a single steady-state that is free of banding artifacts. Another example is cardiovascular imaging, where flow and motion through bands cause transient artifacts.

There are also several possible extensions to this method. The signal and contrast during TR_s is stronger than during TR, and therefore could be useful for improving overall SNR, CNR, and image quality. Low spatial frequency information (which requires shorter readout time) could be acquired during TR_s and somehow combined with full spatial frequency information acquired during TR. It may also be possible to acquire low resolution field maps, coil sensitivity maps, or navigators during the short TR, that can be used to accelerate images or compensate for artifacts.

RF heating is an important constraint for this sequence. Wideband SSFP uses more RF pulses than conventional balanced SSFP for the same amount of readout time. To maintain SAR while using high a-values, the flip angle should be reduced, which may lead to suboptimal SNR or CNR. A possible solution is to use variable rate selective excitation (VERSE) (20) pulses to reduce SAR and permit the use of higher flip angles. If no data is collected during the short-TR, it may also be possible to design RF pulses that combine the $-\alpha$ and α (separated by TR_s) into one composite pulse with lower total SAR than the two separate pulses.

Accelerating the approach to steady state will be important when combining this technique with any type of contrast preparation (e.g. fat saturation or inversion recovery). While a simple method is described in this manuscript, more accurate methods designed for conventional balanced SSFP (15,21,22) may be adapted for use with wideband SSFP. We speculate that magnitude transients during the approach to steady state will be shorter in wideband SSFP compared to conventional balanced SSFP because the magnitude of the steady-state magnetization is closer to M_o (see Fig. 2).

SSFP sequences, in general, are highly sensitive to unbalanced phase. For this reason, phase-encode pairing is used to minimize unbalanced phase caused by gradient distortions (23), and first-moment nulling is used when imaging in areas of flow (11). Although not fully explored at this

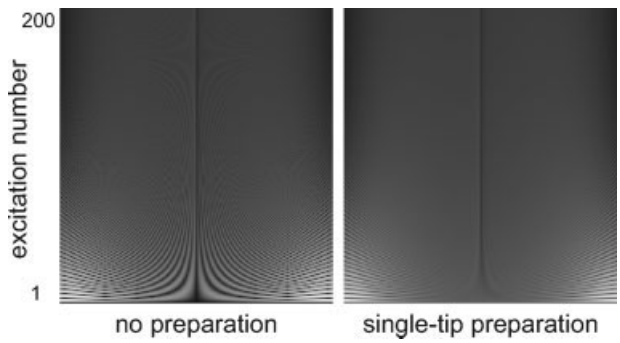

FIG. 8. Initial preparation of wideband SSFP using a single tip. The horizontal axis represents resonance offset and covers the central 2/3 of the null-to-null spacing. The vertical axis is time, and shows the evolution of the signal profile as a function of TR number. Data corresponds to $a = 0.4$, $T_1/T_2 = 1{,}000/300$ ms, TR = 5 ms, $\alpha = 70°$. The preparation consists of single-tip of $+19°$ located TR/2 prior to a $-\alpha$ pulse. Single-tip preparation substantially reduces the amount and duration of transient oscillations.

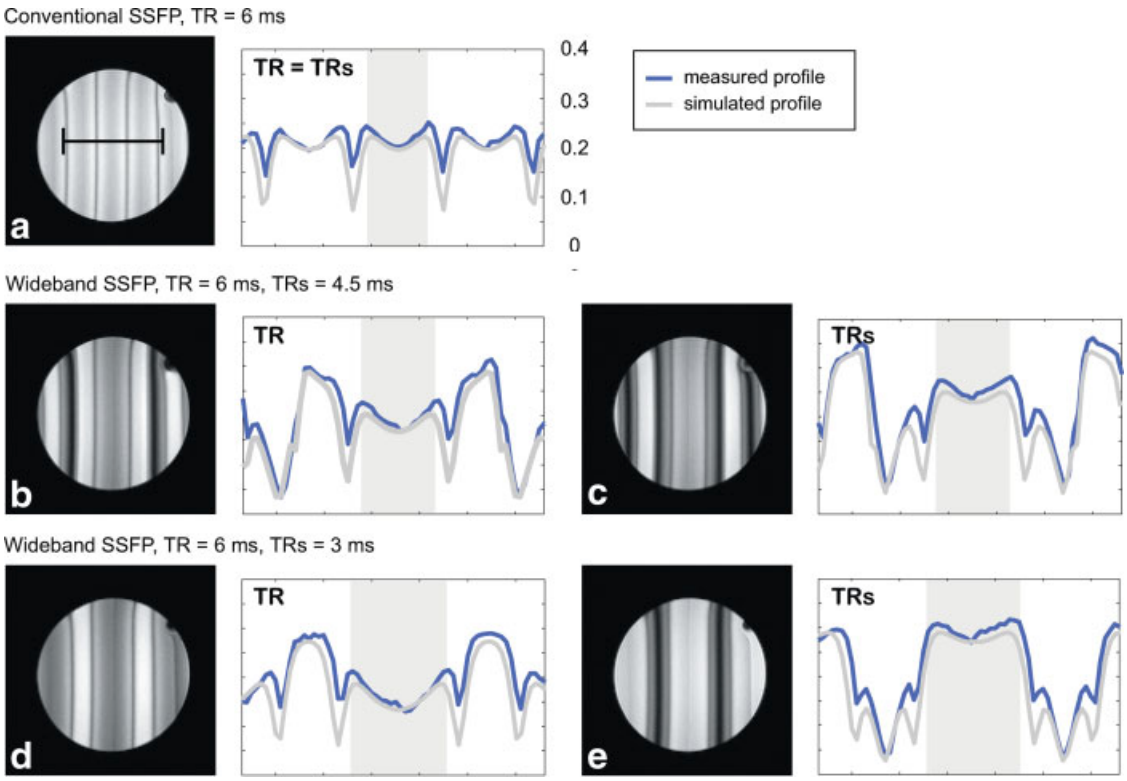

FIG. 9. Measured and simulated signal profiles from a uniform ball phantom with an applied linear shim. Data corresponds to conventional SSFP (**a**) with $a = 1$, and wideband SSFP (**b,c**) with $a = 0.75$ and (**d,e**) with $a = 0.5$. The TR was 6 msec, and flip angle was 30° in all scans. There was excellent agreement in the location of null-bands in simulated and measured profiles. Compared to **a**, the increase in band-spacing in **b** and **c** was 11% and 34% respectively.

time, wideband SSFP and alternating-TR SSFP in general may be more sensitive than conventional SSFP to unbalanced phase due to flow and gradient distortions.

The band-spacing and SNR efficiency of wideband SSFP are influenced by several parameters including the flip angle, α-value, TR, and tissue relaxation times. Optimal tradeoffs may be found experimentally, or by using Bloch simulation (see Fig. 6). When comparing wideband SSFP with conventional single-acquisition SSFP, wideband SSFP is expected to have longer scan-time, and a reduction in pass-band signal during TR, which in some cases will be offset by an increase in available readout duration and/or the use of the echo during TR_s. When comparing wideband SSFP with multiple-acquisition SSFP using phase-cycling, wideband SSFP is expected to have shorter scan-time and lower SNR efficiency.

CONCLUSIONS

We have demonstrated a new technique, called wideband SSFP, that widens the band spacing in single-acquisition balanced SSFP imaging. Simulations indicate that wideband SSFP preserves high SNR efficiency and T_2/T_1 contrast. Phantom studies verified the expected band spacing increase in both available echoes. This technique has been successfully applied to the avoidance of banding artifacts in cine cardiac imaging and high-resolution knee imaging at 3T.

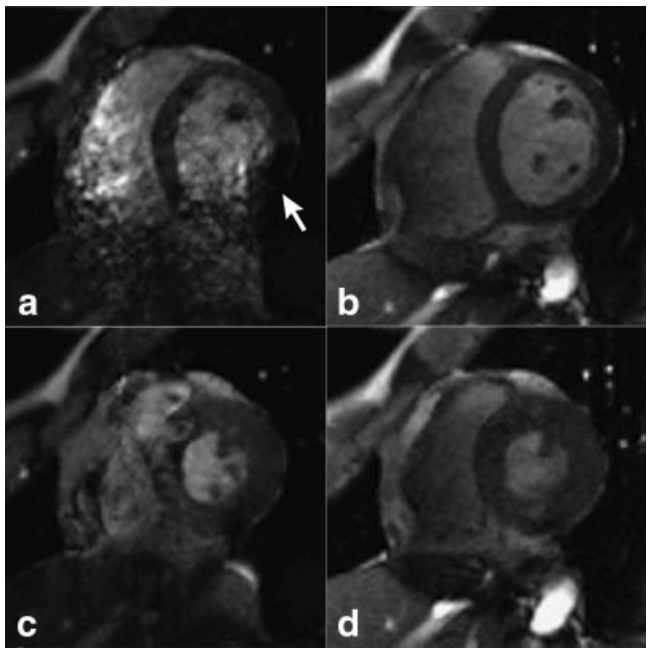

FIG. 10. Cardiac images from a healthy volunteer at 3 Tesla. Short-axis (top) diastolic and (bottom) systolic frames are from breath-held cine acquisitions with 1.2×1.2 mm^2 in-plane resolution using (**a,c**) conventional SSFP with TR = 4.4 msec, and (**b,d**) wideband SSFP with TR_s/TR = 2.0/4.4 msec. Notice the absence of dark bands (white arrow) and flow-related artifacts in the wideband SSFP images.

FIG. 11. Axial knee images from a healthy volunteer at 3 Tesla. (**a**) conventional bSSFP with 0.3×0.3 mm^2 in-plane resolution and TR = 6.8 ms, (**b**) conventional bSSFP with 0.15×0.30 mm^2 in-plane resolution and TR = 10.8 ms, (**c**) wideband SSFP with 0.15×0.30 mm^2 in-plane resolution and TR_s/TR = 2.8/10.8 msec. Wideband SSFP **c** achieves high in-plane resolution while avoiding banding artifacts experienced by conventional SSFP **b** (white arrows and insets). Lipid signal appears different in all three images due to large differences in the signal profiles outside of the on-resonance passband.

Wideband SSFP has a wide range of potential applications. Broadly stated, it enables the use of longer readout durations with a fixed band spacing (for improved spatial resolution and efficient k-space sampling), and enables an increase in the band spacing for a fixed TR (for the avoidance of banding artifacts). Wideband SSFP may be particularly useful for high-resolution balanced SSFP imaging at high-field strengths, due to the increased off-resonance and long required readout durations.

ACKNOWLEDGMENTS

We thank Zungho Zun, Jon-Fredrik Nielsen, Garry Gold, and Gerald Pohost for discussions and collaboration. HLL has received the support of a USC Viterbi School of Engineering Graduate Fellowship.

REFERENCES

1. Carr HY. Steady-state free precession in nuclear magnetic resonance. Phys Rev 1958;112.
2. Oppelt A, Graumann R, Barfuss H, Fischer H, Hartl W, Shajor W. FISP–A new fast MRI sequence. Electromedica 1986;54:15–18.
3. Freeman R, Hill HDW. Phase and intensity anomalies in Fourier transform NMR. J Magan Reson 1971;4:366–383.
4. Zur Y, Stokar S, Bendal P. An analysis of fast imaging seqnences with steady-state transverse magnetization refocusing. Magn Reson Med 1988;6:175–193.
5. Markl M, Alley MT, Elkins CJ, Pelc NJ. Flow effects in balanced steady state free precession imaging. Magn Reson Med 2003;50:892–903.
6. Haacke EM, Wielopolski PA, Tkach JA, Modic MT. Steady-state free precession imaging in the presence of motion: Application for improved visualization of the cerebrospinal fluid. Radiology 1990;175: 545–552.
7. Hinshaw WS. Image formation by nuclear magnetic resonance: the sensitive-point method. J Appl Phys 1976;47:3709–3721.
8. Schär M, Kozerke S, Fischer SE, Boesiger P. Cardiac SSFP imaging at 3 Tesla. Magn Reson Med 2004;51:799–806.
9. Herzka DA, Kellman P, Aletras AH, Guttman MA, McVeigh ER. Multi-shot epi-SSFP in the heart. Magn Reson Med 2002;47:655–664.
10. Slavin GS, Saranathan M. FIESTA-ET: High-resolution cardiac imaging using echo-planar steady-state free precession. Magn Reson Med 2002;48:934–941.
11. Nayak KS, Hargreaves BA, Hu BS, Nishimura DG, Pauly JM, Meyer CH. Spiral balanced SSFP cardiac imaging. Magn Reson Med 2005;53:1468–1473.
12. Leupold J, Hennig J, Scheffler K. Alternating repetition time balanced steady state free precession. Magn Reson Med 2006;55:557–565.
13. Nayak KS, Hu HS, Hargreaves BA. Wideband SSFP:SSFP imaging with bandwidth greater than 1/TR. In: Proceedings of ISMRM, 13th Annual Meeting, Miami; 2005. p 2389.
14. Henning J, Speck O, Scheffler K. Optimization of signal behavior in the transition to driven equilibrium in steady-state free precession sequences. Magn Reson Med 2002;48:801–809.
15. Hargreaves BA, Vasanawala SS, Pauly JM, Nishimura DG. Characterization and reduction of the transient response in steady-state MR imaging. Megn Reson Med 2001;46:149–158.
16. Leupold J, Henning J, Scheffler K. Fast fat saturation for balanced SSFP imaging at low flip angles using alternating TR. In: Proceedings of ISMRM, 12th Annual Meeting, Kyoto; 2004. p 266.
17. Jaynes ET. Matrix treatment of nuclear induction. Phys Rev 1955;98:1099–1105.
18. Schmitt P, Griswold MA, Gulani V, Haase A, Flentje M, Jakob PM. A simple geometrical description of the TrueFISP ideal transient and steady-state signal. Magn Reson Med 2006;55:177–186.
19. Deimling M, Heid O. Magnetization prepared true FISP imaging. In: Proceedings of SMR, 2nd Annual Meeting, Dallas, 1994; p 495.
20. Conolly SM, Nishimura DG, Macovski A, Glover G. Variable-rate selective excitation. J Magn Reson 1988;78:440–458.
21. Nishimura DG, Vasanwala SS. Analysis and reduction of the transient response in SSFP imaging. In: Proceedings of ISMRM, 8th Annual Meeting, Denver, 2000; p 301.
22. LeRoux P. Simplified model and stabilization of SSFP sequences. J Magn Reson 2003;163:23–37.
23. Bieri O, Markl M, Scheffler K. Analysis and compensation of eddy currents in balanced SSFP. Magn Reson Med 2005;54:129–137.